Effect of distance-dependent dispersivity on density-driven flow in porous media

Anis Younes, Marwan Fahs, Behzad Ataie-Ashtiani, Craig T. Simmons

Effect of distance-dependent dispersivity on density-driven flow in porous media

Anis Younes[1,2,3], Marwan Fahs[1], Behzad Ataie-Ashtiani[4,5], Craig T. Simmons[5]

[1] *LHyGES, Univ. de Strasbourg/EOST/ENGEES, CNRS, 1 rue Blessig, 67084 Strasbourg, France.*
[2] *LISAH, Univ Montpellier, INRA, IRD, Montpellier SupAgro, Montpellier, France.*
[3] *LMHE, Ecole Nationale d'Ingénieurs de Tunis, Tunisie*
[4] *Department of Civil Engineering, Sharif University of Technology, PO Box 11155-9313, Tehran, Iran*
[5] *National Centre for Groundwater Research and Training, College of Science and Engineering, Flinders University, GPO Box 2100, Adelaide, SA 5001, Australia*

Submitted to ***Journal of Hydrology***

*Contact person: Marwan Fahs

E-mail : fahs@unistra.fr

Abstract

In this study, the effect of distance-dependent dispersion coefficients on density-driven flow is investigated. The linear asymptotic model, which assumes that dispersivities increase linearly with distance from the source of contamination and reach asymptotic values at a large asymptotic distance, is employed. An in-house numerical model is adapted to handle distance-dependent dispersion. The effect of asymptotic-dispersion on aquifer contamination is analyzed for two tests: (*i*) a seawater intrusion problem in a coastal aquifer and (*ii*) a leachate transport problem from a surface deposit site. Global Sensitivity Analysis (GSA) combined with the Polynomial Chaos Expansion (PCE) surrogate modelling is conducted to assess the influence of the dispersion coefficients on the contamination plume for both configurations.

For the seawater intrusion problem, the results show that the length of the toe is mainly controlled by the asymptotic transverse dispersivity whereas the spread of the concentration is sensitive to the asymptotic longitudinal dispersivity and the asymptotic dispersivity distance. The latter is the most important parameter controlling the amount of salt which intrudes into the aquifer. For the leachate transport problem, the results show that the asymptotic longitudinal dispersivity coefficient does not affect the concentration distribution. The asymptotic dispersivity distance has a strong effect on the total amount of contaminant that enters the aquifer. This effect can be three times more important than the effect of the asymptotic transverse dispersivity. These findings are likely to be helpful for the investigation and management of density-driven flow problems.

Keywords

Density driven flow, saltwater intrusion, leachate transport, variable dispersion, asymptotic model, global sensitivity analysis.

1. Introduction

Density-driven flow (DDF) is a particular configuration of transport in porous media in which the fluid concentration causes a change in groundwater density which can significantly affect the flow dynamics. DDF can be encountered in several applications related to contaminant transport in aquifers. Among these applications, a well-known problem is the contamination of coastal aquifers by saltwater intrusion (Werner et al., 2013) which is a major concern around the world. Another important example is groundwater contamination by leachates from surface industrial waste and landfills (Frind, 1982). Managing and predicting the evolution of pollutants in such situations require accurate numerical simulations.

The simulation of DDF problems is based on coupling Darcy's groundwater flow equation to the solute transport equation via a state relation expressing the density as a function of solute concentration. Transport of solute in the aquifer is ruled by advection, representing the solute displacement by the mean fluid flow, and by dispersion, which accounts for solute spreading caused by velocity variations due to the heterogeneity of the porous medium at different scales (Liu et Kitandis, 2013; Kitanidis, 2017; Dai et al., 2020). Dispersion processes have been found to play a major role in DDF problems as they cause mixing between different fluids. The effect of dispersion on DDF has been widely investigated in the literature. For instance, Abarca et al. (2007) studied the effect of dispersion on DDF in the context of seawater intrusion and showed that when dispersion is taken into account, concentration isolines resemble those observed in real coastal aquifers. Emami-Meybodi (2017) studied instabilities driven by dispersion for an unstable DDF problem with mixed convective flow. Wen et al. (2018) defined a dispersive Rayleigh number and investigated the effect of dispersion on the Rayleigh-Darcy convection problem. Fahs et al. (2020) investigated the effect of dispersion on thermal DDF problem.

In most DDF models, dispersion is ruled using a velocity-dependent dispersion tensor involving constant coefficients characterizing mixing in the longitudinal (parallel to the flow) and

transverse (orthogonal to flow) directions. In the last decades, many studies have shown that this conventional approach cannot satisfactorily represent field transport especially for aquifers with spatial heterogeneity (Pickens and Grisak, 1981a). Alternative approaches have developed such as stochastic models (e.g. Gelhar, 1992; Zhang, 2002, Kerrou and Renard, 2010; Pool et al., 2015) or continuous time random walk methods (e.g. Berkowitz et al., 2000; Dentz et al., 2004). However, these methods usually require sufficient field measurements to formulate statistical structure and are known to be computationally expensive (Wang et al., 2006). Such difficulties have motivated using the conventional dispersion approach, but by considering that the dispersivity values are temporal or scale dependent (Pickens and Grisak, 1981a). In other words, the longitudinal and transverse dispersion coefficients are not constant but can vary with the distance from the source of contamination. Indeed, in a tracer test, Molz et al. (1983) found that dispersivity is not constant but increases with the travel distance because of the scale dependence of dispersivities. This phenomenon has been observed both in field-scale transport (e.g. Pickens and Grisak 1981a; Gelhar et al., 1992; Schulze-Makuch, 2005) and laboratory-scale transport (e.g., Silliman and Simpson, 1987; Khan and Jury, 1990; Huang et al., 1995; Vanderborght and Vereecken, 2007). According to Gao et al. (2012), the scale dependence of dispersivity can be related to different processes such as the heterogeneity of the porous media at different scales (Gelhar et al., 1992; Huang et al., 2006), the fractal nature of the pore space in the aquifer (Wheatcraft and Tyler, 1988) or the anomalous transport (Cortis and Berkowitz, 2004). Mishra and Parker (1990) showed that a hyperbolic dispersivity-distance function allows a good fitting of the data estimated from a natural gradient tracer experiment. Kangle et al. (1996) provided a one-dimensional analytical solution with linear asymptotic dispersion. Chen et al. (2003, 2007) investigated distance-dependent dispersion for convergent and divergent flow fields with linear scale-dependent dispersion. Chen et al (2008a) studied one-dimensional transport with hyperbolic asymptotic dispersivity function. Pérez Guerrero and Skaggs (2010)

derived a general analytical solution for one-dimensional transport with distance-dependent coefficients. Gao et al. (2010, 2012) investigated mobile-immobile transport model with asymptotic scale-dependent dispersivity. You and Zhan (2013) developed semi-analytical solutions for solute transport in a finite column with linear asymptotic and exponential distance-dependent dispersivities and time-dependent sources.

Thus, in the literature, the effect of asymptotic dispersivity has been essentially investigated for simplified situations of 1D transport (e.g. Basha and El-Habel, 1993; Yates, 1992; David-Logan, 1996; Pang and Hunt, 2001; Chen et al., 2003; Pérez Guerrero and Skaggs, 2010; Sharma and Abgaze, 2015, Wang et al., 2019), 2D problems with a uniform flow field (e.g. Hunt, 2002; Chen et al., 2008b) or radially convergent divergent flow fields (e.g. Chen et al., 2003, 2006, 2007). To the best our knowledge, investigation of distance-dependent dispersion coefficients in cases involving complex velocity fields, such as in DDF problems, have not been undertaken.

The aim of this work is to incorporate distance-dependent dispersion in a DDF model and to investigate the effect of dispersion parameters on contaminant transport. As conceptual models, we consider (*i*) the Henry problem describing seawater intrusion (SWI) in a coastal aquifer (Henry, 1964) and (*ii*) the leachate transport problem proposed by Frind (1982) to investigate the leachate plume from a surface deposit site. The effect of distance-dependent dispersivities on the aquifer contamination is investigated using Global Sensitivity Analysis (GSA) combined with Polynomial Chaos Expansion (PCE) surrogate modelling (Sudret, 2008; Fajraoui et al., 2012, 2017; Mara et al., 2017).

2. Methods

2.1 The mathematical model and numerical code

The mathematical model for water movement through porous media is based on the mass conservation equation and Darcy's law (Guevara et al., 2015):

$$\rho S \frac{\partial h}{\partial t} + \varepsilon \frac{\partial \rho}{\partial C} \frac{\partial C}{\partial t} + \rho \nabla \cdot \boldsymbol{q} = 0 \quad (1)$$

$$\boldsymbol{q} = -\frac{\rho_0 g}{\mu} \boldsymbol{k} \left(\nabla h + \frac{\rho - \rho_0}{\rho_0} \nabla z \right) \quad (2)$$

where ρ is the fluid density [ML^{-3}], S the specific mass storativity related to head changes [L^{-1}], h the equivalent freshwater head [L], t the time [T], ε the porosity [-], C the relative concentration [-], $\boldsymbol{q}$ the Darcy's velocity [LT^{-1}], ρ_0 the density of the displaced fluid [ML^{-3}], g the gravity acceleration [LT^{-2}], μ the fluid dynamic viscosity [$ML^{-1}T^{-1}$], $\boldsymbol{k}$ the permeability tensor [L^2] and z the depth [L] taken positive upwards.

The contaminant transport in porous media is based on the solute mass conservation equation:

$$\frac{\partial (\varepsilon \rho C)}{\partial t} + \nabla . (\rho C \boldsymbol{q} - \rho \boldsymbol{D} . \nabla C) = 0 \quad (3)$$

where the dispersive tensor $\boldsymbol{D}$ is given by:

$$\boldsymbol{D} = D_m \boldsymbol{I} + (\alpha_L - \alpha_T) \boldsymbol{q}\boldsymbol{q}^T / |\boldsymbol{q}| + \alpha_T |\boldsymbol{q}| \boldsymbol{I} \quad (4)$$

with α_L and α_T the longitudinal and transverse dispersion coefficients [L], D_m the pore water diffusion coefficient [L^2T^{-1}] and $\boldsymbol{I}$ the unit tensor. The associated boundary conditions of the flow-transport system (1)-(3) are of Dirichlet, Neuman or mixed type.

Flow and transport equations are coupled via the linear mixture density equation:

$$\rho = \rho_0 + (\rho_1 - \rho_0) C \quad (5)$$

where ρ_1 is density of contaminant.

In this work, we assume that the longitudinal and transverse dispersion coefficients are a function of the distance from the source of contamination. Distance-dependent dispersivities are generally ruled using one of the four types of functions suggested by Pickens and Grisak (1981b) including linear, parabolic, asymptotic and exponential functions. The linear distance-dependent dispersivity function has been largely used in the literature (e.g. Pang and Hunt,

2001; Gao et al., 2010; Pérez Guerrero and Skaggs, 2010; Chen et al., 2008b). However, this function seems to be unphysical, because field observations show that a constant dispersivity could be asymptotically reached (Gelhar et al., 1992; Pickens and Grisak, 1981a). Huang et al. (1995) used a linear-asymptotic distance-dependent function where the dispersivity value increases linearly with the transport distance and reaches an asymptotic value at a certain large distance. The linear-asymptotic model was adopted by You and Zhan (2013) and is employed in this work:

$$\alpha_{L,T}\left(\boldsymbol{x}\right)=\begin{cases}\alpha_{L,T}^{0}\dfrac{\ell}{\ell_0}, & 0\le\ell\le\ell_0\\ \alpha_{L,T}^{0}, & \ell_0\le\ell\end{cases} \tag{6}$$

where ℓ corresponds to the distance from the source of contamination, α_L^0 and α_T^0 are respectively the asymptotic longitudinal and transverse dispersion coefficients and ℓ_0 is the asymptotic distance after which both longitudinal and transverse dispersivities reach their asymptotic values $\alpha_{L,T}=\alpha_{L,T}^0$.

The coupled flow-transport system is solved with an advanced in-house numerical model using triangular meshes (Ackerer and Younes, 2008). The flow equations (Eqs. 1-2) are solved by the mixed finite element method (Younes et al., 2010). The transport equation (Eq. 3) is solved by combining two numerical methods: Discontinuous Galerkin (DG) method for solving advection and Multipoint Flux Approximation (MPFA) method for solving dispersion. Coupling between flow and transport equations is performed using the non-iterative scheme proposed in Younes and Ackerer (2010) with proper time management. This scheme was shown to be highly efficient and more accurate than the standard iterative procedure. The in-house code has been validated by comparison against semi-analytical solutions in Fahs et al. (2016). Performance and robustness of the code has been highlighted in Shao et al. (2018) by comparison against COMSOL Multiphysics. In this work, the in-house code is modified to handle distance-

dependent dispersion coefficients. Both longitudinal and transverse dispersivities are defined elementwise and their values are calculated using (Eq. 4) where ℓ corresponds to the distance from the center of each element to the source of contamination.

2.2 The Henry saltwater Intrusion Problem

Real applications of SWI at a field scale are increasingly reported in the literature. However, in several theoretical and applied studies, SWI is often investigated based on the hypothetical Henry problem (Henry, 1964) (Figure 1a). This problem represents a common benchmark that is widely used for multiple purposes as understanding physical processes, numerical model verification, and parameter sensitivity analyses. A detailed review of the different use of the Henry problem as a surrogate representation of SWI can be found in Werner et al. (2013) and Fahs et al. (2018).

The Henry problem represents SWI in a vertical cross-section of a confined coastal aquifer where an inland freshwater flow is in equilibrium with seawater that intrudes into the aquifer from the seaside due to its higher density (Figure 1a). The first studies on the Henry problem have been limited to pure molecular diffusion cases. More realistic configurations that include velocity-dependent dispersion have been suggested in Abarca et al. (2007) and Fahs et al. (2016). These cases will be considered here as this work deals with asymptotic dispersion coefficients.

(a)

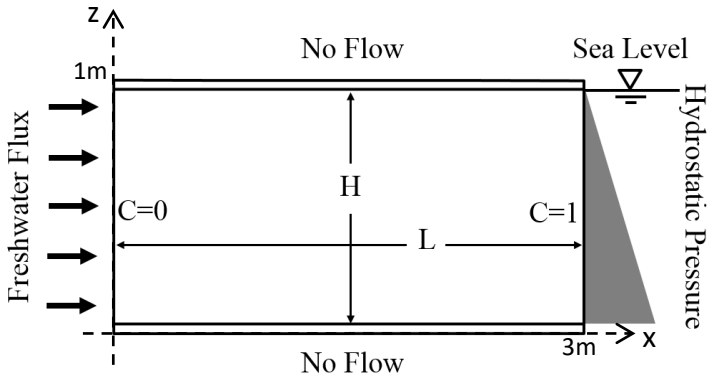

(b)

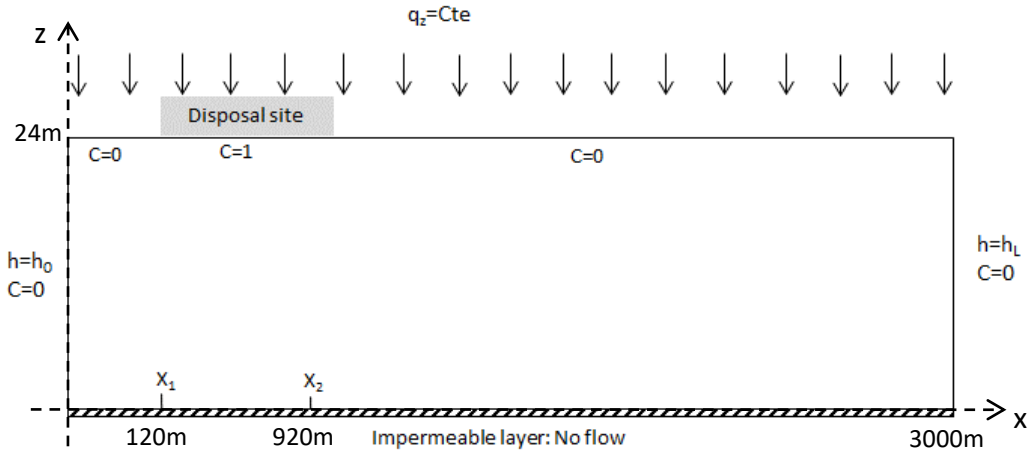

Figure 1. (a) Henry problem domain and boundary conditions; (b) The leachate transport problem (Frind, 1982).

Following Simpson and Clement (2004), we decrease the freshwater recharge by half to increase the density-dependent effects compared to boundary forces. Further, we use a larger rectangular domain with an aspect ratio $\frac{L}{H} = 3$ as proposed by Zidane et al. (2012) to reduce the influence of the left boundary condition on the saltwater distribution. The parameters and boundary conditions for the Henry problem are given in Table 1.

206
207
208
209
210 **Table 1.** Parameters and boundary conditions for the Henry problem.

permeability	k= 1.0204 x 10^{-9} m^2
porosity	$\varepsilon = 0.35$
length of the aquifer	$L = 3$ m
height of the aquifer	$H = 1$ m
-molecular diffusion coefficient	$D_m = 9.4\times10^{-8}$ m^2 s^{-1}
Boundary conditions for flow	- hydrostatic pressure at the right hand side
	- constant flux at the inland boundary: $Q = 3.3\times10^{-5}$ m^2/s
	- no flow along the top and bottom
Boundary conditions for transport	- ρ_0 = 1000 kg/m^3 on the left boundary.
	- ρ_1 = 1025 kg/m^3 on the right boundary
	- zero concentration gradient along the top and bottom

211

212 The numerical model is employed to analyze the saltwater intrusion by considering that
213 uncertainty of model outputs is associated with the following dispersion parameters: the
214 asymptotic longitudinal dispersivity α_L^0, the asymptotic transverse dispersivity α_T^0 and the
215 asymptotic distance ℓ_0. Note that the longitudinal and transverse dispersivities are assumed to
216 be independent. The corresponding uncertainty ranges (Table 2) are sufficiently large to explore
217 the role of each parameter.

218 **Table 2.** Uncertainty ranges of the dispersion coefficients for the Henry problem.

Parameter	Uncertainty Range
α_L^0 [m]	[0.1, 1.0]
α_T^0 [m]	[0.04, 1.0]
ℓ_0 [m]	[0, 2.0]

219

2.3 The leachate transport problem in unconfined aquifer

This problem was proposed by Frind (1982) to investigate groundwater contamination by leachates from sanitary landfills or industrial waste disposal sites. A typical problem is considered (Figure 1b) where a disposal site unprotected from precipitation is situated above the water table in a rectangular unconfined aquifer of 3000 m length and 24m thickness. The parameters and boundary conditions are described in Table 3.

Table 3. Parameters and boundary conditions for the leachate transport problem.

- permeability	k_x= 0.3262 x 10^{-10} m^2
	k_z= 0.3262 x 10^{-11} m^2
- porosity	$\varepsilon = 0.2$
- length of the aquifer	$L = 3000$ m
- height of the aquifer	$H = 24$ m
- molecular diffusion coefficient	$D_m = 0.0\ m^2\ s^{-1}$
- boundary conditions for flow	- fixed head at the left (h_0=*0*) and right (h_L=*-17.5m*) hand sides
	- constant flux at the top: $q_z = 30$ cm/year
	- no flow along the bottom
- boundary conditions for transport	- fixed relative concentration (C=C_0) at the top with
	C_0=1 for $x_1 \le x \le x_2$
	C_0=0 elsewhere
	with $x_1 = 120$ m and $x_2 = 920$ m
	- fixed relative concentration (*C=0*) at the left and right hand sides
	- density of the contaminant $\rho_1 = 1007.1$ kg/m^3
	- zero concentration gradient along the bottom

Large uncertainty ranges (Table 4) are associated to the dispersion parameters (α_L^0, α_T^0 and ℓ_0) in order to investigate the role of each of them. Note that because the leachate transport problem has larger dimensions than the synthetic Henry problem, the dispersion parameters are allowed to have larger values than previously.

234

235 **Table 4.** Uncertainty ranges of the dispersion parameters for the leachate transport problem.

Parameter	Uncertainty Range
α_L^0 [m]	[0.1, 20.0]
α_T^0 [m]	[0.04, 5.0]
ℓ_0 [m]	[0, 50.0]

236

237 ***3.* Global sensitivity analysis**

238 Effect of the dispersion parameters on DDF is investigated using global sensitivity analysis
239 (GSA). To this aim, the variance-based sensitivity indices of Sobol' (Sobol', 2001) are
240 computed using Polynomial Chaos Expansion (PCE). The Sobol' indices measure the
241 contribution of an input (alone or by interactions with other inputs) to the output variance. They
242 are well adapted for GSA since they do not require any assumption of monotony or linearity of
243 the model (Saltelli et al., 2006). Two Sobol' indices are noteworthy:

244 - the first-order sensitivity index,

245 $$S_i = \frac{V\left[E\left[y|\chi_i\right]\right]}{V\left[y\right]} = \frac{V_i}{V} \tag{4}$$

246 - the total sensitivity index,

247 $$ST_i = \frac{E\left[V\left[y|\boldsymbol{\chi}_{-i}\right]\right]}{V\left[y\right]} = \frac{V_i^T}{V} \tag{5}$$

248 where y is the model output, $\boldsymbol{\chi}$ is the set of parameters $\boldsymbol{\chi} = \left(\alpha_L^0, \alpha_T^0, \ell_0\right)$, $E[\ ]$ is the
249 mathematical expectation (the average), $V[\ ]$ is the mathematical variance, $E[\ |\ ]$ and $V[\ |\ ]$
250 are their respective conditional forms. χ_i represents one of the parameters, and $\boldsymbol{\chi}_{-i}$ stands for
251 the set of parameters $\boldsymbol{\chi}$ without the parameter χ_i.

The first-order sensitivity index (or main effect index) $S_i \in [0,1]$ measures the amount by which the variance of *y* is reduced when the true value of χ_i is known. The total sensitivity index $ST_i \in [0,1]$ measures the remaining uncertainty in *y* after all parameters are known except χ_i. It evaluates the contribution of χ_i to the response variance, including its interactions with the other parameters (i.e., $\boldsymbol{\chi}_{\sim i}$). If interactions between parameters are negligible, we have $\sum_i S_i = 1$ and $S_i = ST_i$, $\forall i$.

The marginal effect $\bar{y}(\chi_i)$ of the parameter χ_i on the model output y enables to investigate the range of variation of y with respect to χ_i,

$$\bar{y}(\chi_i) = E\left[y \middle| \chi_i \right]. \tag{7}$$

In this work, we use the Polynomial Chaos Expansion (PCE) surrogate modeling to infer sensitivity indices (Fajraoui et al., 2012, 2017; Younes et al., 2016; Shao et al., 2017). PCE allows an efficient evaluation of the Sobol' indices, since they can be easily calculated using the PCE coefficients (Sudret, 2008).

Since we deal with only three uncertain parameters (α_L^0, α_T^0 and ℓ_0), we use a full surrogate PCE of order 4. The number of polynomial coefficients in the expansion is therefore $\frac{7!}{4! \times 3!} = 35$. The coefficients of the surrogate PCE are calculated by a least-square technique minimizing the sum of squared errors between model responses and the PCE. To this aim, a hundred of evaluations of the Henry and leachate transport problems are performed using parameter values randomly generated in the intervals of variation given in Table 2 and Table 4 respectively.

4. Results for the Henry SWI problem

A mesh converged solution is obtained a uniform triangular mesh formed by 4800 elements. The effect of the dispersion parameters on saltwater intrusion is investigated based on the following metrics (see Figure 2).

- The positions $X_{0.1}, X_{0.5}$ and $X_{0.9}$ of respectively the 10%, 50% and 90% isochlors at the aquifer bottom. Note that the $X_{0.5}$ is related to the well-known length of the toe L_{toe} which is the distance between the seaside boundary and $X_{0.5}$.
- The spread of the concentration $L_S = X_{0.9} - X_{0.1}$ which corresponds to the distance between the 10% and the 90% isochlors at the bottom of the domain.
- The total mass in the domain.
- The values of steady state concentration at the following selected points: $A_1(1.5,0)$; $A_2(2.5,0)$ and $A_3(2.5,1)$.

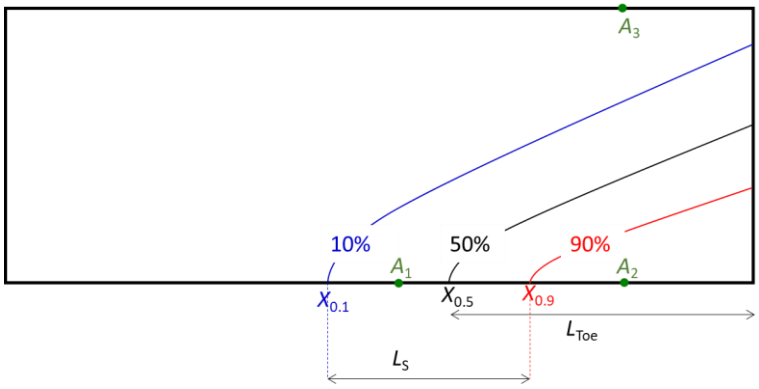

Figure 2. Seawater intrusion metrics used for the assessment of effects of the dispersion parameters.

4.*1 Salinity distribution*

Figure 3a depicts the mean concentration values as well as the corresponding 10%, 50% and 90% concentration contours. This figure shows that the distribution of the mean concentration reflects the general distribution of salinity in coastal aquifers which gives confidence to the accuracy of the PCE surrogate model. Saltwater intrudes from the right and reaches equilibrium

with the inland freshwater flow. Saltwater intrusion is more pronounced near the bottom because of density effects. The mean concentration distribution in Figure 3a shows a wide mixing zone due to the large uncertainty ranges of the dispersion parameters (Table 2).

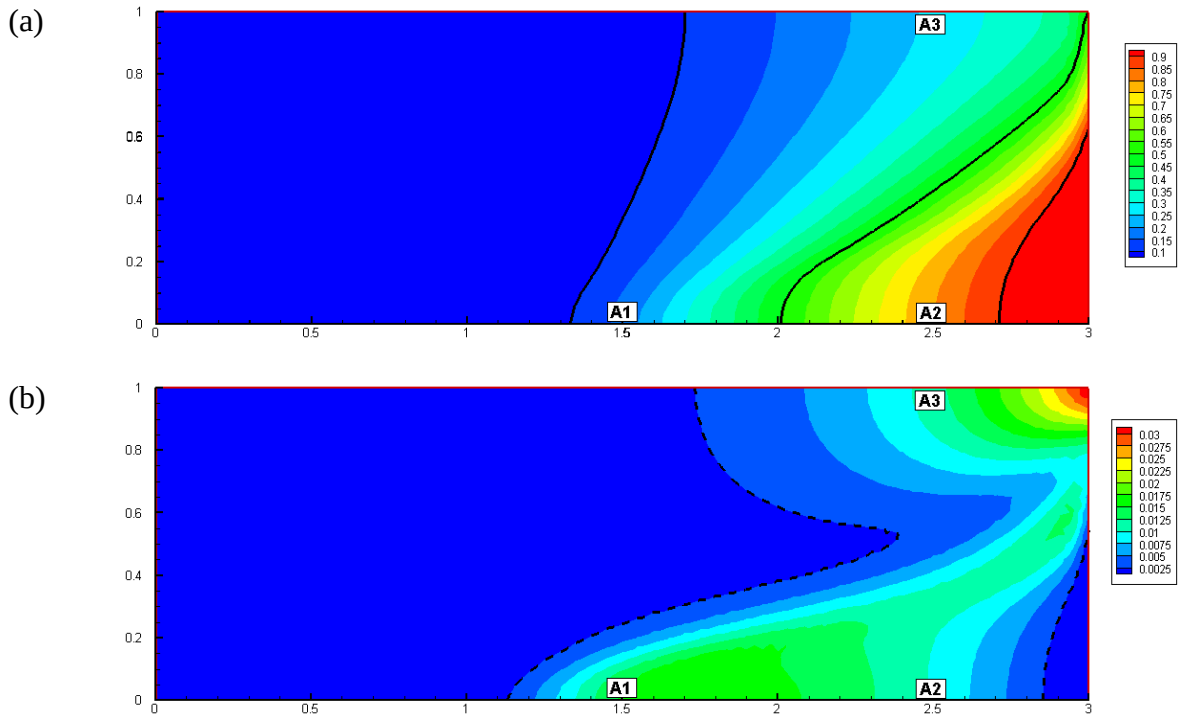

Figure 3. The Henry problem: (a) Spatial map of the mean concentration values (black lines represent 90%, 50% and 10% isochlors); (b) Spatial map of the variance of concentrations (dashed lines limit the zone of high variability- 5% of standard deviation).

The distribution of the variance of the concentration shows that high variances regions are located at the center of the domain near the bottom of the aquifer (Figure 3b). This makes sense as the length of the toe is mainly controlled by the dispersion processes (Abarca et al., 2007; Fahs et al., 2016). Indeed, it is well known that low dispersion increases the buoyancy forces compared to dispersion effects and yields much more intrusion near the bottom of the aquifer (Younes and Fahs, 2014). This explains the high variance region near A1 in Figure 3b. Significant variability of the salinity can be observed also at top of the aquifer near the seaside (Figure 3b). In this zone, the groundwater flow is discharging to the sea. Thus, the salinity of

this zone is mainly due to dispersion. The dashed contour in Figure 3b shows the region where the effect of dispersion parameters is significant which corresponds to 5% of the standard deviation of the concentrations.

The spatial maps of first order Sobol' indices representing the sensitivity of the salinity distribution to α_L^0, α_T^0 and ℓ_0 are plotted in the Figure 4. For the region of significant variance (the region delimited by the dashed lines), Figure 4a shows that α_L^0 has a negligible effect on salinity distribution, except around A2 where a moderate effect can be observed. The parameter α_T^0 is the most influential parameter as its zone of high sensitivity is situated in the region of high variability (Figure 4b). Significant sensitivity to α_T^0 is observed around A3 but the highest sensitivity area is situated in the mixing zone near A1. This is in agreement with the results of Fahs et al. (2016) and is related to the fact that in this zone, the velocity field is not parallel to the concentration gradient. As shown in Fahs et al. (2016), in such a case, the dispersion processes are dominated by the transverse dispersion and hence, the salinity distribution is highly sensitive to α_T^0 in this zone. The parameter ℓ_0 is influential near the seaside boundary (Figure 4c) which makes sense since, far from the sea, the longitudinal and transverse dispersion coefficients reach their asymptotic values and the salinity distribution become insensitive to ℓ_0 .

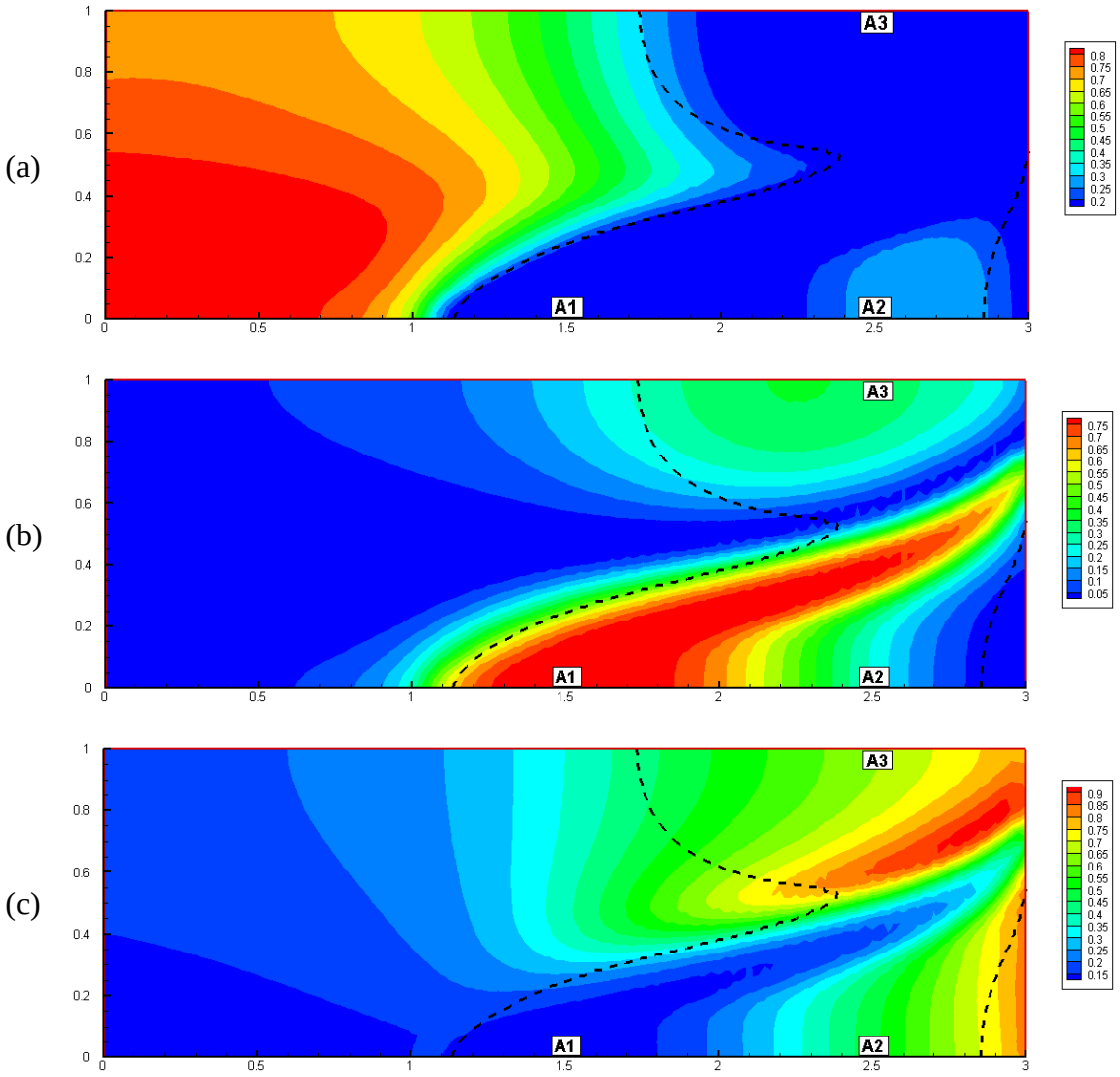

Figure 4. Spatial maps of the first-order sensitivity indices: (a) sensitivity of salinity distribution to α_L^0, (b) sensitivity of salinity distribution to α_T^0 and (c) sensitivity of salinity distribution to ℓ_0. Dashed lines limit the zone of high variability (5% of standard deviation).

4.2 Sensitivity of the SWI metrics

The Sobol' indices for the concentration at the observation points (A1, A2, A3) as well as for the SWI metrics are depicted in Table 5. This table also gives the mean value and the standard deviation for all quantities of interest.

Table 5. Sensitivity of the concentration at the observation points (A1, A2 and A3) and of the SWI metrics. S_1, S_2 and S_3 represent the first order Sobol' indices for the sensitivity to

343 α_L^0, α_T^0 and ℓ_0. 'mean' and 'std' represent the mean value and the standard deviation for the
344 quantities of interest.
345

	mean	**std**	S_1	S_2	S_3	$\sum_{i=1}^{3} S_i$
A1	0.17	0.12	0.01	0.81	0.04	0.86
A2	0.79	0.1	0.27	0.24	0.42	0.94
A3	0.27	0.11	0.02	0.33	0.6	0.95
$X_{0.1}$	1.39	0.17	0.13	0.64	0.06	0.82
$X_{0.5}$	2.0	0.19	0.07	0.73	0.13	0.93
$X_{0.9}$	2.66	0.19	0.30	0.16	0.46	0.93
L_S	1.27	0.23	0.5	0.05	0.41	0.97
Total mass	1016	110	0.16	0.16	0.35	0.67

346

347 The results of this table show that

348 - The concentration near A1 is mostly influenced by α_T^0 $\left(S_2 = 0.81\right)$. In this region,
349 moderate interactions occur between parameters $\left(\sum_{i=1}^{3} S_i = 0.86\right)$. The effects of α_L^0 and
350 ℓ_0 alone are insignificant $\left(S_2 = 0.01 \text{ and } S_3 = 0.04\right)$, but their total effects (including
351 interactions) are moderately significant $\left(ST_1 = 0.12 \text{ and } ST_3 = 0.11\right)$. The results around
352 A1 are coherent with the results discussed previously based on the spatial maps of
353 Sobol' indices (Figure 4).
354 - Around A2, located near the sea boundary, high concentrations can be observed
355 (mean=0.79). The concentration has slight variability (std=0.1) which indicates that
356 SWI reaches this point whatever the values of the dispersion parameters. The most
357 influential parameter near A2 is ℓ_0 $\left(S_3 = 0.42\right)$. The parameters α_L^0 and α_T^0 have

significant and close effects $(S_1 = 0.27$ and $S_2 = 0.24)$. Interactions between dispersion parameters are not significant $\left(\sum_{i=1}^{3} S_i = 0.94\right)$.

- The point A3 is located near the top of the domain and close to the sea boundary. The standard deviation (std=0.11) of concentrations is relatively significant (mean=0.27). The most influential parameter in this region is ℓ_0 $(S_3 = 0.6)$ followed by the parameter α_T^0 $(S_2 = 0.33)$. The parameter α_L^0 is irrelevant $(S_1 = 0.02)$. Interactions between the three dispersion parameters are not significant $\left(\sum_{i=1}^{3} S_i = 0.95\right)$.

- The 10% isochlor intersects the substratum at an average distance of 1.39 m from the sea boundary. $X_{0.1}$ has high variability (std=0.17m). The parameter α_T^0 is the most influential parameter $(S_2 = 0.64)$. The parameter α_L^0 has a small first order sensitivity index $(S_1 = 0.13)$ whereas the parameter ℓ_0 has a negligible first order sensitivity index $(S_3 = 0.06)$. However, because of interaction between parameters $\left(\sum_{i=1}^{3} S_i = 0.82\right)$, α_L^0 and ℓ_0 are influential since their total sensitivity indices are significant $(ST_1 = 0.29$ and $ST_2 = 0.2)$.

- The 50% isochlor intersects the substratum at an average distance of 2.0 m. The dispersion parameters have a strong effect on that position since the standard deviation is significant (std=0.19). As $X_{0.1}$, $X_{0.5}$ is mainly controlled by the parameter α_T^0 $(S_2 = 0.73)$. The parameters α_L^0 $(S_1 = 0.07)$ and ℓ_0 $(S_3 = 0.13)$ have a limited effect. Because the 50% isochlor is closer to the sea than the 10% isochlor, $X_{0.5}$ is more sensitive to ℓ_0 than $X_{0.1}$. Small interactions are observed between the dispersion

parameters $\left(\sum_{i=1}^{3} S_i = 0.93\right)$. Therefore, $X_{0.5}$ and in consequence L_{toe} are mainly controlled by the asymptotic transverse dispersivity. Since interactions are small, the marginal effect of α_T^0, depicted in the Figure 5a, reflects the behavior of $X_{0.5}$ when varying α_T^0 (the other parameters are set at their mean values). Figure 5a shows a high sensitivity for $\alpha_T^0 \leq 0.3$ and a weaker sensitivity for higher values of α_T^0. In this figure, $X_{0.5}$ increases with α_T^0 which is consistent with physics as the decrease in α_T^0 induces more saltwater intrusion and hence a decrease of $X_{0.5}$.

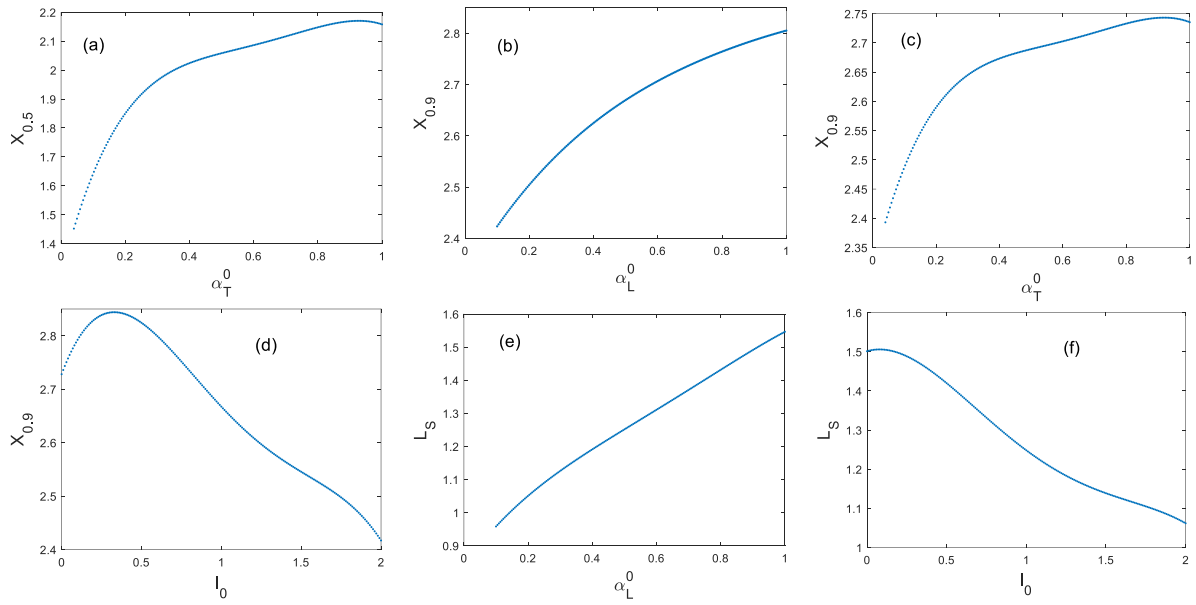

Figure 5. Marginal effect of: (a) α_T^0 on $X_{0.5}$, (b) α_L^0 on $X_{0.9}$, (c) α_T^0 on $X_{0.9}$, (d) ℓ_0 on $X_{0.9}$, (e) α_L^0 on L_S and (f) ℓ_0 on L_S

- The 90% isochlor intersects the substratum at an average distance of 2.66 m with a standard deviation of 0.19 m. $X_{0.9}$ is sensitive to the three dispersion parameters. As the isochlor 90% is close to the sea, the most influential parameter is ℓ_0 $(S_3 = 0.46)$, comes next α_L^0 $(S_1 = 0.30)$ and finally α_T^0 $(S_2 = 0.16)$. Small interactions exist between the

dispersion parameters $\left(\sum_{i=1}^{3} S_i = 0.93\right)$. Marginal effects of the three sensitive dispersion parameters on $X_{0.9}$ are plotted in the Figure 5. The sensitivity of $X_{0.9}$ to α_L^0 (Figure 5b) has a positive slope as an increase of α_L^0 induces an increase of the spreading of the concentration front resulting in an increase of $X_{0.9}$. The sensitivity of $X_{0.9}$ to α_T^0 (Figure 5c) is similar to that observed for $X_{0.5}$. This demonstrates that saltwater intrusion is mainly controlled by the asymptotic transverse dispersivity. A decrease of α_T^0 induces more intrusion which results in a decrease of $X_{0.5}$ and $X_{0.9}$. The sensitivity of the intrusion to α_T^0 is more pronounced for small values of this parameter. The $X_{0.9}$ varies almost linearly with a negative slope with respect to the parameter ℓ_0 (Figure 5d). Indeed, the 90% isochlor is located near the sea boundary (the average $X_{0.9}$ is 2.66m) where the effect of ℓ_0 is significant (see Figure 4c). In that region, the increase of ℓ_0 yields less dispersion effects which results in more saltwater intrusion and hence a decrease in $X_{0.9}$.

- For the spread of the concentration (L_S), the most influential parameter is α_L^0 $\left(S_1 = 0.5\right)$, followed by ℓ_0 $\left(S_3 = 0.41\right)$. The sensitivity of L_S to α_L^0 is much more important than that of $X_{0.1}$ and $X_{0.9}$. Furthermore, although α_T^0 is influential on $X_{0.9}$ and on $X_{0.1}$, it has no effect on L_S $\left(S_2 = 0.05\right)$. The interactions between parameters are almost absent $\left(\sum_{i=1}^{3} S_i = 0.97\right)$. The marginal effects of the parameters α_L^0 and ℓ_0 on L_S are depicted in the Figure 5. L_S increases linearly with the value of α_L^0 (Figure 5e). This confirms that the spreading is directly proportional to the value of α_L^0. The sensitivity of L_S to

412 ℓ_0 has a negative slope (Figure 5f). The increase of ℓ_0 yields less dispersion which
413 results in less spreading of the concentration front and hence a reduction in L_S.

414 - The standard deviation of the total mass in the aquifer is around 10% of its mean value.
415 Significant interactions occur between the dispersion parameters $\left(\sum_{i=1}^{3} S_i = 0.67\right)$. The
416 total sensitivity indices of the three dispersion parameters $\left(ST_1 = 0.46,\ ST_2 = 0.23\right.$ and
417 $\left.ST_3 = 0.64\right)$ are significantly higher than their first order indices $\left(S_1 = 0.16,\ S_2 = 0.16\right.$
418 and $\left.S_3 = 0.35\right)$. This shows that ℓ_0 plays the most important role on the amount of mass
419 which has intruded into the domain, followed by α_L^0. Strong interactions mainly occur
420 between these two parameters since $ST_3 - S_3 = 0.29$ and $ST_1 - S_1 = 0.3$ whereas
421 $ST_2 - S_2 = 0.07$.

422 **5. Results of the leachate transport problem**

423 Starting with no leachate in the aquifer, the leachate transport problem is simulated for 24 years.
424 A mesh converged solution is obtained using a uniform triangular mesh formed by 14400
425 triangular elements. A hundred simulations were performed using independent random
426 parameter values generated inside the intervals given in Table 4. The mean leachate plume is
427 shown in the Figure 6a. The leachate enters the aquifer due to dispersion and vertical infiltration.
428 Within the aquifer, the leachate plume moves to the right side due to the hydraulic gradient
429 between left and right sides. A stable flow is obtained for all explored dispersivity values
430 because of (*i*) the large dispersion and (*ii*) the weak density difference between the contaminant
431 and freshwater.
432
433
434

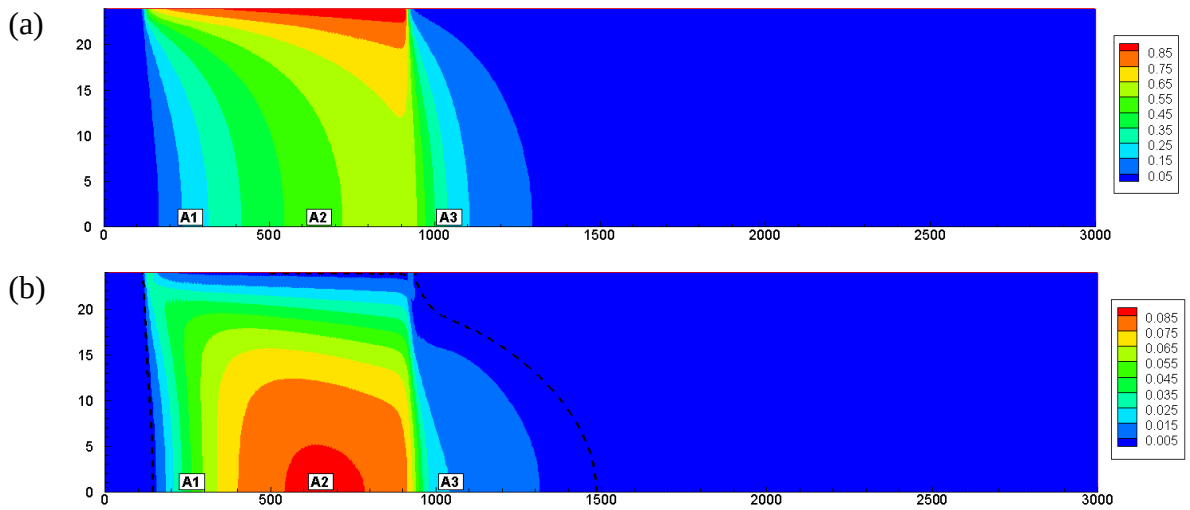

435

436 **Figure 6.** The leachate transport problem at 24 years: (a) Spatial map of the mean concentration
437 values and (b) Spatial map of variance of concentration. The dashed contour delimits the region
438 of high variances (5% of standard deviation).
439

440 The distribution of the variance of the concentration shows that high variability is located below
441 the disposal site (Figure 6b) towards the bottom of the aquifer. The center of the zone of high
442 variability is shifted to the right of the disposal site center because of the basic advective flow
443 in the aquifer which goes from left to right.

444 Figure 7 shows the spatial distributions of the first-order Sobol' indices. For the region of
445 significant variability (delimited by dashed lines), the asymptotic longitudinal dispersivity α_L^0
446 has a negligible first-order sensitivity index (Figure 7a). Note that this does not imply the
447 irrelevance of α_L^0 since the first-order index does not take into account interactions between
448 parameters. To judge the inefficiency of α_L^0, we evaluate the total Sobol index of α_L^0. Figure
449 8 shows that, in the region of high variance, α_L^0 has no effect on the concentration distribution
450 (neither alone nor in interaction with the other parameters). Therefore, the parameter α_L^0 is
451 irrelevant for concentration distribution. Thus, in this case, mixing by dispersion is mainly
452 related to transverse dispersivity. The parameters α_T^0 and ℓ_0 have strong influence on the
453 concentration distribution (Figure 7b and 7c) in the region of high variability (below the landfill

454 site). Significant interactions are observed between these two parameters. The amount of
455 interaction between parameters can be evaluated by computing $r = 1 - \sum_i S_i$. If interactions
456 between parameters are absent, then $\sum_i S_i = 1$ and $r = 0$. Figure 9 shows that interactions
457 between α_T^0 and ℓ_0 are observed in two regions located in the lower half of domain. Moderate
458 interactions occur in the region between x = 100 m and x = 500 m. Higher interactions occur in
459 a larger zone located downstream the deposit site between x = 1000 m and x = 1500m.
460
461
462
463

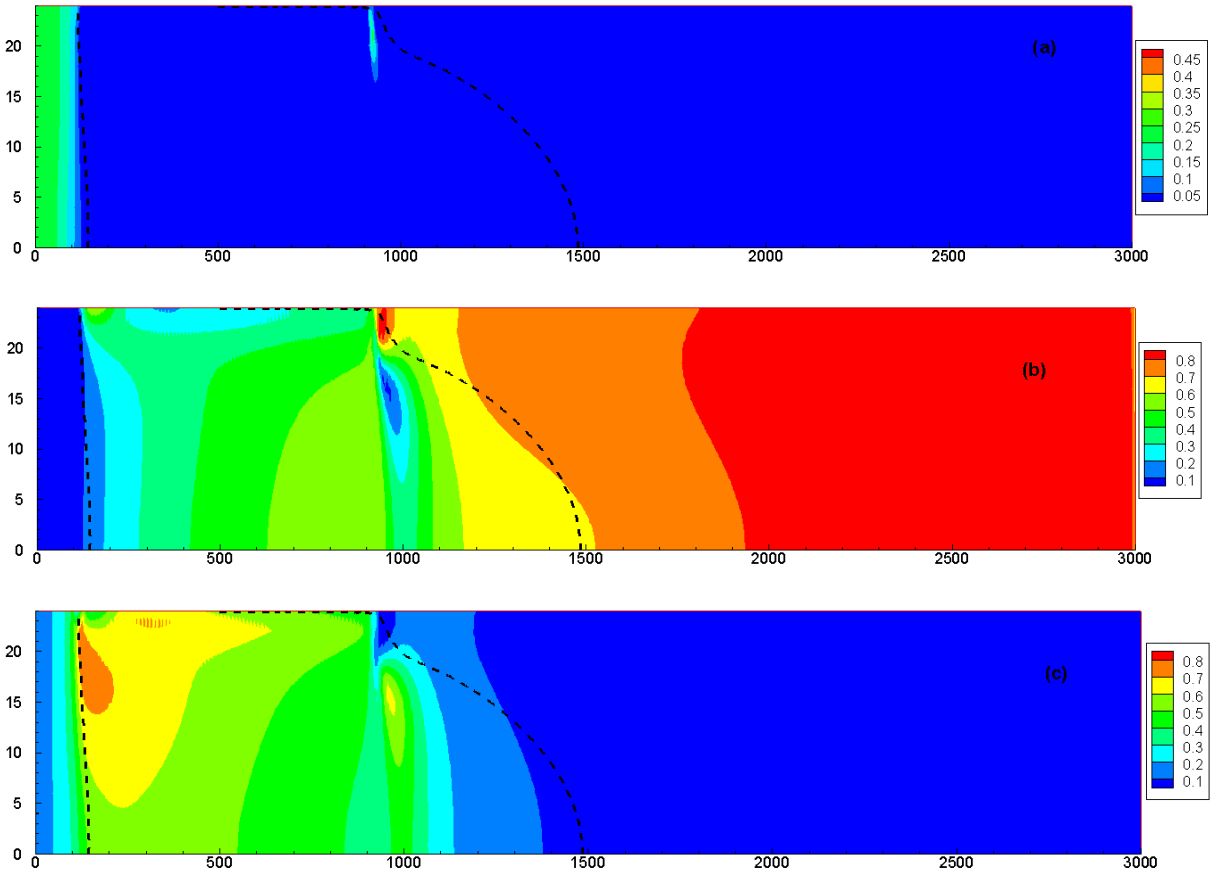

464 **Figure 7.** Spatial map of the first order sensitivity indices for the leachate transport problem:
465 a) sensitivity to α_L^0, b) sentitivity to α_T^0 and c) sensitivity to ℓ_0.

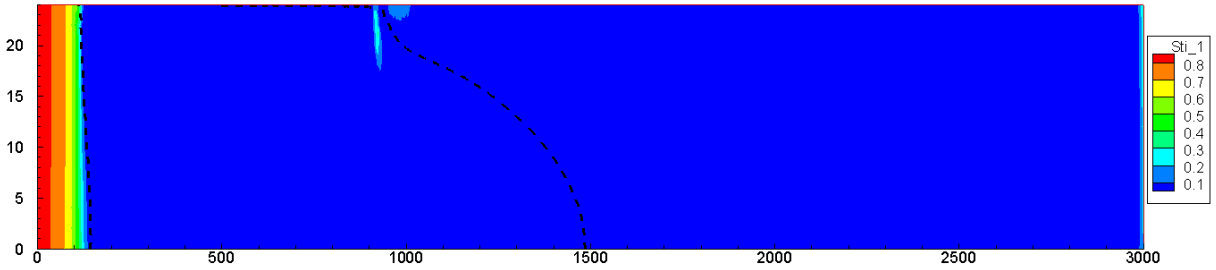

Figure 8. Spatial map of the total Sobol' index of α_L^0 for the leachate transport problem.

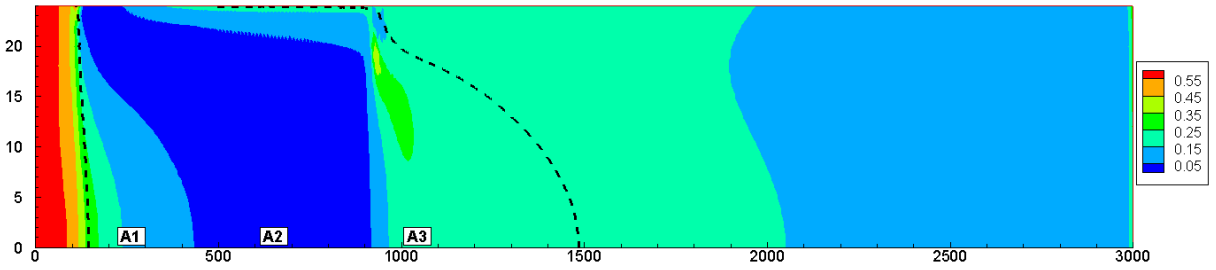

Figure 9. Spatial map of the interaction $r = 1 - \sum_i S_i$ for the leachate transport problem.

The effects of dispersion parameters are investigated for the total mass in the domain and for the final concentration at the following selected points $A_1(265,0)$; $A_2(655,0)$ and $A_3(1025,0)$ in Table 6. The results of this table show that:

	mean	std	S_1	S_2	S_3	$\sum_{i=1}^{3} S_i$
A1	0.19	0.2	0.0	0.29	0.58	0.87
A2	0.52	0.3	0.	0.51	0.46	0.97
A3	0.29	0.13	0.0	0.37	0.39	0.76
Total mass	10667	4058	0.0	0.24	0.74	0.98

Table 6. Sobol's indices for the concentration at the observation points ($A_{1,..,3}$) and for the total mass in the domain for the leachate transport problem. S_1, S_2 and S_3 represent the first order Sobol' indices for the sensitivity to α_L^0, α_T^0 and ℓ_0. 'mean' and 'std' represent the mean value and the standard variation for the quantities of interest.

- The concentration around A1 is first influenced by ℓ_0 $(S_3 = 0.58)$ and then by α_T^0 $(S_2 = 0.29)$. The parameter α_L^0 is irrelevant $(ST_1 = 0)$. Moderate interactions occur between α_L^0 and ℓ_0 $\left(\sum_{i=1}^{3} S_i = 0.87\right)$.

- The concentration around A2 is almost equally influenced by α_T^0 $(S_2 = 0.51)$ and ℓ_0 $(S_3 = 0.46)$. In this region, the model is almost additive since interactions between parameters are almost absent $\left(\sum_{i=1}^{3} S_i = 0.97\right)$.

- Around A3, the parameters α_T^0 and ℓ_0 have close first-order sensitivity indices $(S_2 = 0.37$ and $S_3 = 0.39)$ and close total sensitivity indices $(ST_2 = 0.6$ and $ST_3 = 0.63)$. In this region, strong interactions occur between these two parameters $\left(\sum_{i=1}^{3} S_i = 0.76\right)$.

- The total mass in the system has a mean of 10,667 and a significant variance of 4,058. The parameter α_L^0 has no effect $(S_1 = 0)$. The parameter ℓ_0 has a strong effect on the total mass value. This effect $(S_3 = 0.74)$ is three times more important than the effect of α_T^0 $(S_2 = 0.24)$. The effects of the two parameters are additive since interactions between them are almost absent $\left(\sum_{i=1}^{3} S_i = 0.98\right)$. The marginal effects of the parameters α_T^0 and ℓ_0 on the total mass are plotted in Figure 10. The sensitivity of the total mass to α_T^0 depicts a curve with a positive slope since the total mass increases as α_T^0 increases. The marginal effect of ℓ_0 is represented by a negative slope curve which is consistent with physics. The leachate plume, and consequently the total mass, increase as dispersion increases (*i.e.* ℓ_0 decreases).

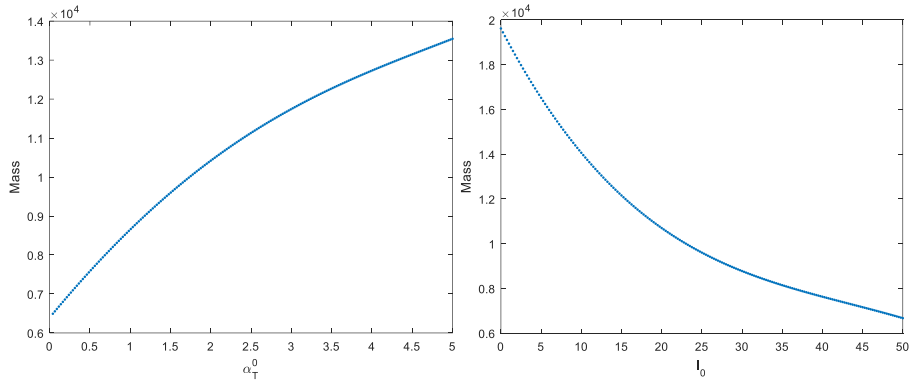

Figure 10. Marginal effects of α_T^0, and ℓ_0 on the total mass for the leachate transport problem.

6. Conclusions

Transport of pollutants in aquifers is usually modeled using the advection-dispersion transport equation with constant-dispersion coefficients. Recently, laboratory and field transport observations have shown that dispersivities are distance-dependent. The most popular function for distance-dependent dispersivity is the linear-asymptotic model which assumes that the longitudinal and transverse dispersion coefficients increase linearly with the distance from the source of contamination until some asymptotic distance ℓ_0, after which the dispersion coefficients reach asymptotic values. In the literature, this model has been investigated in simple configurations dealing with either one-dimensional or uniform two-dimensional flow fields. In this work, we investigate the effects of asymptotic dispersion model in the case of contaminant transport with DDF that involves complex velocity field. The linear-asymptotic model has been incorporated in an advanced in-house DDF numerical model. The new developed code was used to investigate the effect of the dispersion coefficients (asymptotic longitudinal dispersivity α_L^0, asymptotic transverse dipersivity α_T^0 and asymptotic distance ℓ_0) on the contamination plume for two conceptual models: the Henry saltwater intrusion problem and a leachate transport problem from a surface deposit site. The effects of dispersion parameters are evaluated using Global Sensitivity Analysis (GSA) combined with the

520 Polynomial Chaos Expansion (PCE) surrogate modelling to compute both first-order and total
521 Sobol' sensitivity indices
522 The results for the Henry problem showed that the concentration at the center bottom of the
523 domain, is mostly influenced by the asymptotic value of the transverse dispersion α_T^0 whereas,
524 near the sea boundary, the most influential parameter is the asymptotic distance ℓ_0. The
525 position of the 50% isochlor is mainly controlled by the parameter α_T^0. The spread of the
526 concentration is not influenced by α_T^0 but by α_L^0 and ℓ_0. The total amount of mass intruded in
527 the aquifer is influenced by ℓ_0 and then by α_L^0 and interactions between them.
528 The results for the leachate transport problem show that α_L^0 has no effect (neither alone nor in
529 interaction with the other parameters) on the concentration distribution. The parameters α_T^0
530 and ℓ_0 have a strong influence on the concentration distribution below the landfill site. Strong
531 interactions occur between these two parameters in the aquifer. The total mass in the aquifer is
532 strongly influenced by ℓ_0. The sensitivity to ℓ_0 is three times more important than to α_T^0 and
533 the effects of these two parameters on the total mass are additive (interactions are insignificant).
534 This study showed that distance-dependent dispersion coefficients can significantly affect
535 contaminant distribution in aquifers in the case of density-driven flow. It demonstrates the
536 advantage of using GSA with PCE surrogate modeling for such investigation since it allows to
537 determine, for each parameter, the regions of high influence and the regions where the effect of
538 the parameter is insignificant. It also allows to determine regions of high interactions between
539 parameters and to explore the marginal effect of sensitive parameters on the model output.
540
541
542
543

Acknowledgments

This work was partially supported by the Tunisian-French joint international laboratory NAILA (http://www.lmi-naila.com/). Marwan Fahs would acknowledge the support from the national school of water and environmental engineering of Strasbourg through the research project PORO6100. Behzad Ataie-Ashtiani and Craig T. Simmons acknowledge support from the National Centre for Groundwater Research and Training, Australia. Behzad Ataie-Ashtiani also appreciates the support of the Research Office of the Sharif University of Technology, Iran. The data used in this work are available on the GitHub repository: https://github.com/fahs-LHYGES

References

1. Abarca, E., Carrera, J., Sánchez-Vila, X., & Dentz, M. (2007). Anisotropic dispersive Henry problem. *Advances in Water Resources*, *30*(4), 913–926. https://doi.org/10.1016/j.advwatres.2006.08.005
2. Ackerer, P., & Younes, A. (2008). Efficient approximations for the simulation of density driven flow in porous media. *Advances in Water Resources*, *31*(1), 15–27. https://doi.org/10.1016/j.advwatres.2007.06.001
3. Basha, H. A., & El-Habel, F. S. (1993). Analytical solution of the one-dimensional time-dependent transport equation. *Water Resources Research*, *29*(9), 3209–3214. https://doi.org/10.1029/93WR01038
4. Berkowitz, B., Scher, H., Silliman, S.E., 2000. Anomalous transport in laboratory-scale, heterogeneous porous media. Water Resour. Res. 36, 149–158. https://doi.org/10.1029/1999WR900295
5. Chen, J.-S., Liu, C.-W., Hsu, H.-T., & Liao, C.-M. (2003). A Laplace transform power series solution for solute transport in a convergent flow field with scale-dependent dispersion. *Water Resources Research*, *39*(8). https://doi.org/10.1029/2003WR002299
6. Chen, J.-S., Liu, C.-W., & Liang, C.-P. (2006). Evaluation of longitudinal and transverse dispersivities/distance ratios for tracer test in a radially convergent flow field with scale-dependent dispersion. *Advances in Water Resources*, *29*(6), 887–898. https://doi.org/10.1016/j.advwatres.2005.08.001
7. Chen, J.-S., Chen, C.-S., & Chen, C. Y. (2007). Analysis of solute transport in a divergent flow tracer test with scale-dependent dispersion. *Hydrological Processes*, *21*(18), 2526–2536. https://doi.org/10.1002/hyp.6496
8. Chen, J.-S., Ni, C.-F., Liang, C.-P., & Chiang, C.-C. (2008a). Analytical power series solution for contaminant transport with hyperbolic asymptotic distance-dependent dispersivity. *Journal of Hydrology*, *362*(1–2), 142–149. https://doi.org/10.1016/j.jhydrol.2008.08.020
9. Chen, J.-S., Ni, C.-F., & Liang, C.-P. (2008b). Analytical power series solutions to the two-dimensional advection-dispersion equation with distance-dependent dispersivities. *Hydrological Processes*, *22*(24), 4670–4678. https://doi.org/10.1002/hyp.7067
10. Cortis, A., & Berkowitz, B. (2004). Anomalous Transport in "Classical" Soil and Sand Columns. *Soil Science Society of America Journal*, *68*(5), 1539–1548. https://doi.org/10.2136/sssaj2004.1539
11. Dai, Z., Zhan, C., Dong, S., Yin, S., Zhang, X., & Soltanian, M. R. (2020). How does resolution of sedimentary architecture data affect plume dispersion in multiscale and hierarchical systems? *Journal of Hydrology*, *582*, 124516. https://doi.org/10.1016/j.jhydrol.2019.124516
12. David Logan, J. (1996). Solute transport in porous media with scale-dependent dispersion and periodic boundary conditions. *Journal of Hydrology*, *184*(3–4), 261–276. https://doi.org/10.1016/0022-1694(95)02976-1
13. Dentz, M., Cortis, A., Scher, H., Berkowitz, B., 2004. Time behavior of solute transport in heterogeneous media: transition from anomalous to normal transport. Advances in Water Resources 27, 155–173. https://doi.org/10.1016/j.advwatres.2003.11.002
14. Emami-Meybodi, H. (2017). Dispersion-driven instability of mixed convective flow in porous media. *Physics of Fluids*, *29*(9), 094102. https://doi.org/10.1063/1.4990386
15. Fahs, M., Ataie-Ashtiani, B., Younes, A., Simmons, C. T., & Ackerer, P. (2016). The Henry problem: New semianalytical solution for velocity-dependent dispersion. *Water Resources Research*, *52*(9), 7382–7407. https://doi.org/10.1002/2016WR019288
16. Fahs, M., Koohbor, B., Belfort, B., Ataie-Ashtiani, B., Simmons, C., Younes, A., &

Ackerer, P. (2018). A Generalized Semi-Analytical Solution for the Dispersive Henry Problem: Effect of Stratification and Anisotropy on Seawater Intrusion. *Water*, *10*(2), 230. https://doi.org/10.3390/w10020230

17. Fahs, M., Graf, T., Tran, T. V., Ataie-Ashtiani, B., Simmons, Craig. T., & Younes, A. (2020). Study of the Effect of Thermal Dispersion on Internal Natural Convection in Porous Media Using Fourier Series. *Transport in Porous Media*, *131*(2), 537–568. https://doi.org/10.1007/s11242-019-01356-1
18. Fajraoui, N., Mara, T. A., Younes, A., & Bouhlila, R. (2012). Reactive Transport Parameter Estimation and Global Sensitivity Analysis Using Sparse Polynomial Chaos Expansion. *Water, Air, & Soil Pollution*, *223*(7), 4183–4197. https://doi.org/10.1007/s11270-012-1183-8
19. Fajraoui, Noura, Fahs, M., Younes, A., & Sudret, B. (2017). Analyzing natural convection in porous enclosure with polynomial chaos expansions: Effect of thermal dispersion, anisotropic permeability and heterogeneity. *International Journal of Heat and Mass Transfer*, *115*, 205–224. https://doi.org/10.1016/j.ijheatmasstransfer.2017.07.003
20. Frind, E. O. (1982). Simulation of long-term transient density-dependent transport in groundwater. *Advances in Water Resources*, *5*(2), 73–88. https://doi.org/10.1016/0309-1708(82)90049-5
21. Gao, G., Zhan, H., Feng, S., Fu, B., Ma, Y., & Huang, G. (2010). A new mobile-immobile model for reactive solute transport with scale-dependent dispersion. *Water Resources Research*, *46*(8). https://doi.org/10.1029/2009WR008707
22. Gao, G., Zhan, H., Feng, S., Fu, B., & Huang, G. (2012). A mobile–immobile model with an asymptotic scale-dependent dispersion function. *Journal of Hydrology*, *424–425*, 172–183. https://doi.org/10.1016/j.jhydrol.2011.12.041
23. Gelhar, L. W., Welty, C., & Rehfeldt, K. R. (1992). A critical review of data on field-scale dispersion in aquifers. *Water Resources Research*, *28*(7), 1955–1974. https://doi.org/10.1029/92WR00607
24. Guevara Morel, C. R., van Reeuwijk, M., & Graf, T. (2015). Systematic investigation of non-Boussinesq effects in variable-density groundwater flow simulations. *Journal of Contaminant Hydrology*, *183*, 82–98. https://doi.org/10.1016/j.jconhyd.2015.10.004
25. Henry, H. R. (1964). Effects of dispersion on salt encroachment in coastal aquifers, *1613–C*, 70–84.
26. Huang, G., Huang, Q., & Zhan, H. (2006). Evidence of one-dimensional scale-dependent fractional advection–dispersion. *Journal of Contaminant Hydrology*, *85*(1–2), 53–71. https://doi.org/10.1016/j.jconhyd.2005.12.007
27. Huang, K., Toride, N., & Van Genuchten, M. Th. (1995). Experimental investigation of solute transport in large, homogeneous and heterogeneous, saturated soil columns. *Transport in Porous Media*, *18*(3), 283–302. https://doi.org/10.1007/BF00616936
28. Hunt, B. (2002). Scale-Dependent Dispersion from a Pit. *Journal of Hydrologic Engineering*, *7*(2), 168–174. https://doi.org/10.1061/(ASCE)1084-0699(2002)7:2(168)
29. Kangle, H., van Genuchten, M. T., & Renduo, Z. (1996). Exact solutions for one-dimensional transport with asymptotic scale-dependent dispersion. *Applied Mathematical Modelling*, *20*(4), 298–308. https://doi.org/10.1016/0307-904X(95)00123-2
30. Kerrou, J., Renard, P., 2010. A numerical analysis of dimensionality and heterogeneity effects on advective dispersive seawater intrusion processes. Hydrogeol J 18, 55–72. https://doi.org/10.1007/s10040-009-0533-0
31. Khan, A. U.-H., & Jury, W. A. (1990). A laboratory study of the dispersion scale effect in column outflow experiments. *Journal of Contaminant Hydrology*, *5*(2), 119–131. https://doi.org/10.1016/0169-7722(90)90001-W
32. Kitanidis, P. K. (2017). Teaching and communicating dispersion in hydrogeology, with

emphasis on the applicability of the Fickian model. *Advances in Water Resources*, *106*, 11–23. https://doi.org/10.1016/j.advwatres.2017.01.006
33. Liu, Y., & Kitanidis, P. K. (2013). A mathematical and computational study of the dispersivity tensor in anisotropic porous media. *Advances in Water Resources*, *62*, 303–316. https://doi.org/10.1016/j.advwatres.2013.07.015
34. Mara, T. A., Belfort, B., Fontaine, V., & Younes, A. (2017). Addressing factors fixing setting from given data: A comparison of different methods. *Environmental Modelling & Software*, *87*, 29–38. https://doi.org/10.1016/j.envsoft.2016.10.004
35. Mishra, S., & Parker, J. C. (1990). Analysis of solute transport with a hyperbolic scale-dependent dispersion model. *Hydrological Processes*, *4*(1), 45–57. https://doi.org/10.1002/hyp.3360040105
36. Molz, F. J., Guven, O., & Melville, J. G. (1983). An Examination of Scale-Dependent Dispersion Coefficients. *Ground Water*, *21*(6), 715–725. https://doi.org/10.1111/j.1745-6584.1983.tb01942.x
37. Pang, L., & Hunt, B. (2001). Solutions and verification of a scale-dependent dispersion model. *Journal of Contaminant Hydrology*, *53*(1–2), 21–39. https://doi.org/10.1016/S0169-7722(01)00134-6
38. Pérez Guerrero, J. S., & Skaggs, T. H. (2010). Analytical solution for one-dimensional advection–dispersion transport equation with distance-dependent coefficients. *Journal of Hydrology*, *390*(1–2), 57–65. https://doi.org/10.1016/j.jhydrol.2010.06.030
39. Pickens, J. F., & Grisak, G. E. (1981a). Modeling of scale-dependent dispersion in hydrogeologic systems. *Water Resources Research*, *17*(6), 1701–1711. https://doi.org/10.1029/WR017i006p01701
40. Pickens, J. F., & Grisak, G. E. (1981b). Scale-dependent dispersion in a stratified granular aquifer. *Water Resources Research*, *17*(4), 1191–1211. https://doi.org/10.1029/WR017i004p01191
41. Pool, M., Post, V.E.A., Simmons, C.T., 2015. Effects of tidal fluctuations and spatial heterogeneity on mixing and spreading in spatially heterogeneous coastal aquifers. Water Resour. Res. 51, 1570–1585. https://doi.org/10.1002/2014WR016068
42. Saltelli, A., Ratto, M., Tarantola, S., & Campolongo, F. (2006). Sensitivity analysis practices: Strategies for model-based inference. *Reliability Engineering & System Safety*, *91*(10–11), 1109–1125. https://doi.org/10.1016/j.ress.2005.11.014
43. Schulze-Makuch, D. (2005). Longitudinal dispersivity data and implications for scaling behavior. *Ground Water*, *43*(3), 443–456. https://doi.org/10.1111/j.1745-6584.2005.0051.x
44. Shao, Q., Younes, A., Fahs, M., & Mara, T. A. (2017). Bayesian sparse polynomial chaos expansion for global sensitivity analysis. *Computer Methods in Applied Mechanics and Engineering*, *318*, 474–496. https://doi.org/10.1016/j.cma.2017.01.033
45. Shao, Q., Fahs, M., Hoteit, H., Carrera, J., Ackerer, P., & Younes, A. (2018). A 3-D Semianalytical Solution for Density-Driven Flow in Porous Media. *Water Resources Research*, *54*(12). https://doi.org/10.1029/2018WR023583
46. Sharma, P. K., & Abgaze, T. A. (2015). Solute transport through porous media using asymptotic dispersivity. *Sadhana*, *40*(5), 1595–1609. https://doi.org/10.1007/s12046-015-0382-6
47. Silliman, S. E., & Simpson, E. S. (1987). Laboratory evidence of the scale effect in dispersion of solutes in porous media. *Water Resources Research*, *23*(8), 1667–1673. https://doi.org/10.1029/WR023i008p01667
48. Simpson, M. J., & Clement, T. P. (2004). Improving the worthiness of the Henry problem as a benchmark for density-dependent groundwater flow models. *Water Resources Research*, *40*(1). https://doi.org/10.1029/2003WR002199
49. Sobol′, I. M. (2001). Global sensitivity indices for nonlinear mathematical models and their

Monte Carlo estimates. *Mathematics and Computers in Simulation*, *55*(1–3), 271–280. https://doi.org/10.1016/S0378-4754(00)00270-6
50. Sudret, B. (2008). Global sensitivity analysis using polynomial chaos expansions. *Reliability Engineering & System Safety*, *93*(7), 964–979. https://doi.org/10.1016/j.ress.2007.04.002
51. Vanderborght, J., & Vereecken, H. (2007). Review of Dispersivities for Transport Modeling in Soils. *Vadose Zone Journal*, *6*(1), 29–52. https://doi.org/10.2136/vzj2006.0096
52. Wang, H., Persaud, N., Zhou, X., 2006. Specifying Scale-dependent Dispersivity in Numerical Solutions of the Convection-Dispersion Equation. Soil Sci. Soc. Am. J. 70, 1843–1850. https://doi.org/10.2136/sssaj2005.0166
53. Wang, Q., Gu, H., Zhan, H., Shi, W., & Zhou, R. (2019). Mixing Effect on Reactive Transport in a Column with Scale Dependent Dispersion. *Journal of Hydrology*, 124494. https://doi.org/10.1016/j.jhydrol.2019.124494
54. Wen, B., Chang, K. W., & Hesse, M. A. (2018). Rayleigh-Darcy convection with hydrodynamic dispersion. *Physical Review Fluids*, *3*(12), 123801. https://doi.org/10.1103/PhysRevFluids.3.123801
55. Werner, A. D., Bakker, M., Post, V. E. A., Vandenbohede, A., Lu, C., Ataie-Ashtiani, B., et al. (2013). Seawater intrusion processes, investigation and management: Recent advances and future challenges. *Advances in Water Resources*, *51*, 3–26. https://doi.org/10.1016/j.advwatres.2012.03.004
56. Wheatcraft, S. W., & Tyler, S. W. (1988). An explanation of scale-dependent dispersivity in heterogeneous aquifers using concepts of fractal geometry. *Water Resources Research*, *24*(4), 566–578. https://doi.org/10.1029/WR024i004p00566
57. Yates, S. R. (1992). An analytical solution for one-dimensional transport in porous media with an exponential dispersion function. *Water Resources Research*, *28*(8), 2149–2154. https://doi.org/10.1029/92WR01006
58. You, K., & Zhan, H. (2013). New solutions for solute transport in a finite column with distance-dependent dispersivities and time-dependent solute sources. *Journal of Hydrology*, *487*, 87–97. https://doi.org/10.1016/j.jhydrol.2013.02.027
59. Younes, A., Delay, F., Fajraoui, N., Fahs, M., & Mara, T. A. (2016). Global sensitivity analysis and Bayesian parameter inference for solute transport in porous media colonized by biofilms. *Journal of Contaminant Hydrology*, *191*, 1–18. https://doi.org/10.1016/j.jconhyd.2016.04.007
60. Younes, Anis, & Ackerer, P. (2010). Empirical versus time stepping with embedded error control for density-driven flow in porous media. *Water Resources Research*, *46*(8). https://doi.org/10.1029/2009WR008229
61. Younes, Anis, & Fahs, M. (2014). A semi-analytical solution for saltwater intrusion with a very narrow transition zone. *Hydrogeology Journal*, *22*(2), 501–506. https://doi.org/10.1007/s10040-014-1102-8
62. Younes, Anis, Ackerer, P., & Delay, F. (2010). Mixed finite elements for solving 2-D diffusion-type equations. *Reviews of Geophysics*, *48*(1), RG1004. https://doi.org/10.1029/2008RG000277
63. Zhang, D., 2002. Stochastic methods for flow in porous media: coping with uncertainties. Academic, San Diego, Calif. : London.
64. Zidane, A., Younes, A., Huggenberger, P., & Zechner, E. (2012). The Henry semianalytical solution for saltwater intrusion with reduced dispersion. *Water Resources Research*, *48*(6). https://doi.org/10.1029/2011WR011157

753